LOW RESOLUTION RAINFALL ESTIMATIONS FROM PASSIVE MICROWAVE RADIOMETERS

Dong-Bin Shin

Department of Atmospheric Sciences, Yonsei University, E-mail: dbshin@yonsei.ac.kr

ABSTRACT Analyses of Tropical Rainfall Measuring Mission (TRMM) microwave radiometer (TMI) and precipitation radar (PR) data show that the rainfall inhomogeneity, represented by the coefficient of variation, decreases as rain rate increases at the low resolution (the footprint size of TMI 10 GHz channel). The rainfall inhomogeneity, however, is relatively constant for all rain rates at the high resolution (the footprint size of TMI 37 GHz channel). Consequently, radiometric signatures at lower spatial resolutions are characterized by larger dynamic range and smaller variability than those at higher spatial resolution. Based on the observed characteristics, this study develops a low-resolution (~ 40 x 40 km) rainfall retrieval algorithm utilizing realistic rainfall distributions in the *a-priori* databases. The purpose of the low-resolution rainfall algorithm is to make more reliable climatological rainfalls from various microwave sensors, including low-resolution radiometers.

KEY WORDS: Precipitation Retrievals, Passive Microwave Radiometers

1. INTRODUCTION

Global cloud information has been collected by microwave, infrared and visible sensors from low Earth orbiting and geostationary satellites. Among the sensors, the overwhelming advantage of microwave radiometry in cloud transmission properties for measuring the blackbody emission from cloud columns has been successfully demonstrated in rainfall estimations. In particular, frequencies below ~30 GHz are well suited for detecting rainfalls over ocean since the emission signals from raindrops are clearly separated from the ocean surface by their significant emissivity differences.

Moreover, lower frequency channels from microwave sensors are essential elements for better rainfall retrievals because they have larger dynamic range in the radiometric signals as well as greater ability to penetrate into the rain layers than higher frequency channels. Microwave sensors, however, have relatively large field of view's (FOV's), especially at the lower frequency channels. The large FOV can lead to the so-called "beam-filling" error which is due to the combined effect of the rainfall variability within the sensor FOV and the non-linear response of microwave brightness temperature (T_b) to rain rate (R). A number of investigators such as Chiu et al. (1990), Short and North (1990), and Kummerow (1996) studied the issues regarding the error. The impact of the rainfall inhomogeneity on passive microwave rainfall retrievals should still be investigated with more realistic rain fields.

The successful operation of the TRMM satellite for almost a decade provides space/time rainfall field information at both the regional and global scales. Based on the observed rainfall characteristics, this study examines how prior knowledge on realistic distributions of the rainfall variability can increase the accuracy of rainfall retrievals, especially at low spatial resolutions. In response to the need of a global algorithm, a parametric approach has been developed by Shin and Kummerow (2003; hereafter SK) for rainfall retrieval from various microwave sensors. This type of algorithm is designed to produce homogeneous rainfall estimates from a variety of radiometers being considered for Global Precipitation Misson (GPM) which is a planned international precipitation measuring mission using multiple satellites. The parametric retrieval seemed to produce unbiased rainfall results for a variety of radiometers when the *a-priori* databases were constructed for the appropriate region and time. Using the parametric approach from SK this study develops a rainfall retrieval algorithm at "low" spatial resolutions. Possibly low resolution rainfall retrievals can also lead to participation of radiometers with low resolution FOVs in GPM. As an example, this examines the Advanced Technology Microwave Sounder (ATMS), a 22-channel passive microwave radiometer with a swath width of 2300 km, which is one of the sensors for the planned National Polar Orbiting Operational Environmental Satellite System (NPOESS) Preparatory Project (NPP) satellite, as a possible GPM constellation satellite.

2. OBSERVATIONAL CHARACTERISTICS OF RAIN FIELDS

2.1 Data used

The TRMM microwave imager (TMI) measures upwelling microwave radiances (brightness temperatures) emitted by the Earth and atmosphere at the five frequencies, 10.7, 19.4, 21.3, 37.0 and 85.5 GHz with horizontal and vertical polarizations (only vertical polarization at 21.3 GHz). At each frequency the FOVs are determined by the satellite altitude, antenna size and beam width. The effective FOV at 10.7 GHz is 63 km by

37 km (down-track and cross-track direction). At frequencies of (19.4, 21.3, 37.0 and 85.5 GHz, the FOVs are 30 x 18 km, 23 x 18 km, 16 x 9 km and 7 x 5 km, respectively. The TRMM precipitation radar (PR) operates at 13.8 GHz and measures the return power with a vertical spacing of 250 m for normal samples at a nadir resolution of ~ 4 km and a swath width of 215 km.

This study used the version 6 TMI brightness temperatures (TRMM product number 1B11) and Precipitation Radar (PR) data (2A23 and 2A25) acquired from the National Aeronautics and Space Administration Goddard Space Flight Center Distributed Active Archive Center (NASA/GSFC/DAAC). The PR operates at 13.8 GHz and has a nadir resolution of ~ 4 km (the specification of the pre TRMM boost period). The PR rainfall data are averaged over the three grid box sizes corresponding to FOVs of the TMI's 10.7, 19.4, and 37.0 GHz channel. As a demonstration of concept, analyses are carried out over sections of the east Pacific (0° N ~ 15° N, 130° W ~ 100° W) and the west Pacific (0° N ~ 15° N, 135.5° E ~ 165.5° E) during the period of December 1999 to February 2000 (DJF, 1999-2000).

2.2 Empirical T_b-R relations at different spatial resolutions

Figure 1 shows the T_b-R relations at the high and low spatial resolutions (FOV_{37} and FOV_{10}) for the east and west Pacific. The T_b at the 10.7 GHz-H channel to R relations for the two resolutions are shown in the upper panels (Figure 1a, b). The rainfall data at the PR pixels (~ 4 km) are averaged over the two FOV's. The T_b data at the channel of 10.7 GHz are used directly for FOV_{10}. The 10.7 GHz T_b data at the resolution of FOV_{37} are obtained at every fourth pixels of 37.0 GHz to avoid oversampling of overlapped 10.7 GHz T_b data. For both regions, the T_b's at FOV_{10} are slightly lower than those at FOV_{37} at the low rain rates (below 3 - 4 mm/h) but higher above these rain rates. If a homogeneous rainfall is involved at FOV_{10} and FOV_{37}, the two FOV's should have an equivalent T_b. As such, it seems that the actual distribution of the rainfall inhomogeneity contributes to a greater dynamic range of T_b responses at FOV_{10} than at FOV_{37}. The lower panels represent the relationships between T_b at 19 GHz-H channel and R at the same resolutions (Figure 1c, d) and demonstrate similar results. We can also see that the variability of T_b's, as indicated by the error bars, is smaller at the larger FOV. The same T_b-R relations over the FOV_{19} (not shown) are located in between those for the two resolutions (FOV_{37} and FOV_{10}).

In physically-based rainfall algorithms, the desired inference depends heavily upon the prior knowledge of the radiometric response. For this reason, when cloud-radiative transfer model simulations are used to establish *a-priori* information, it is important to have the prior information as close to nature as possible for better representation of precipitation fields. The decreasing dynamic ranges resulted from the use of lower resolution T_b at the higher resolution, as indicated by solid lines in Figure 1, however, shows that the observation, which would be ideal *a-priori* information, itself includes the imperfectness of the relationships between radiometric signatures and rainfalls resulting from the nature of precipitation with the limit of current sensors' resolution. As such the uncertainty should be considered as an inherent error that can not be solved by improving *a-priori* information from better cloud-radiative transfer models. The improved models would reduce only the differences between the simulated and observed fields, but the uncertainties in the radiometric signatures due to precipitation variability remain intact.

On the other hand, the radiometric signatures from the lower resolution channels convolved at the lower resolution (FOV_{10}), indicated by dotted lines in Figure 1, are characterized by the larger dynamic range and smaller variability than at the higher resolution (FOV_{37}). It may imply that the low resolution rainfall estimates can have less systematic bias than the high resolution estimates if the actual rainfall distribution is accounted for in the retrievals. The low resolution rainfall estimates are not capable of describing the details of instantaneous rainfalls. The smaller bias can, however, propagate through averaging process to obtain the climatological estimates. In order to demonstrate this effect, this study performs rainfall retrievals at different retrieval resolutions based on the observed T_b and rainfall databases in the following section.

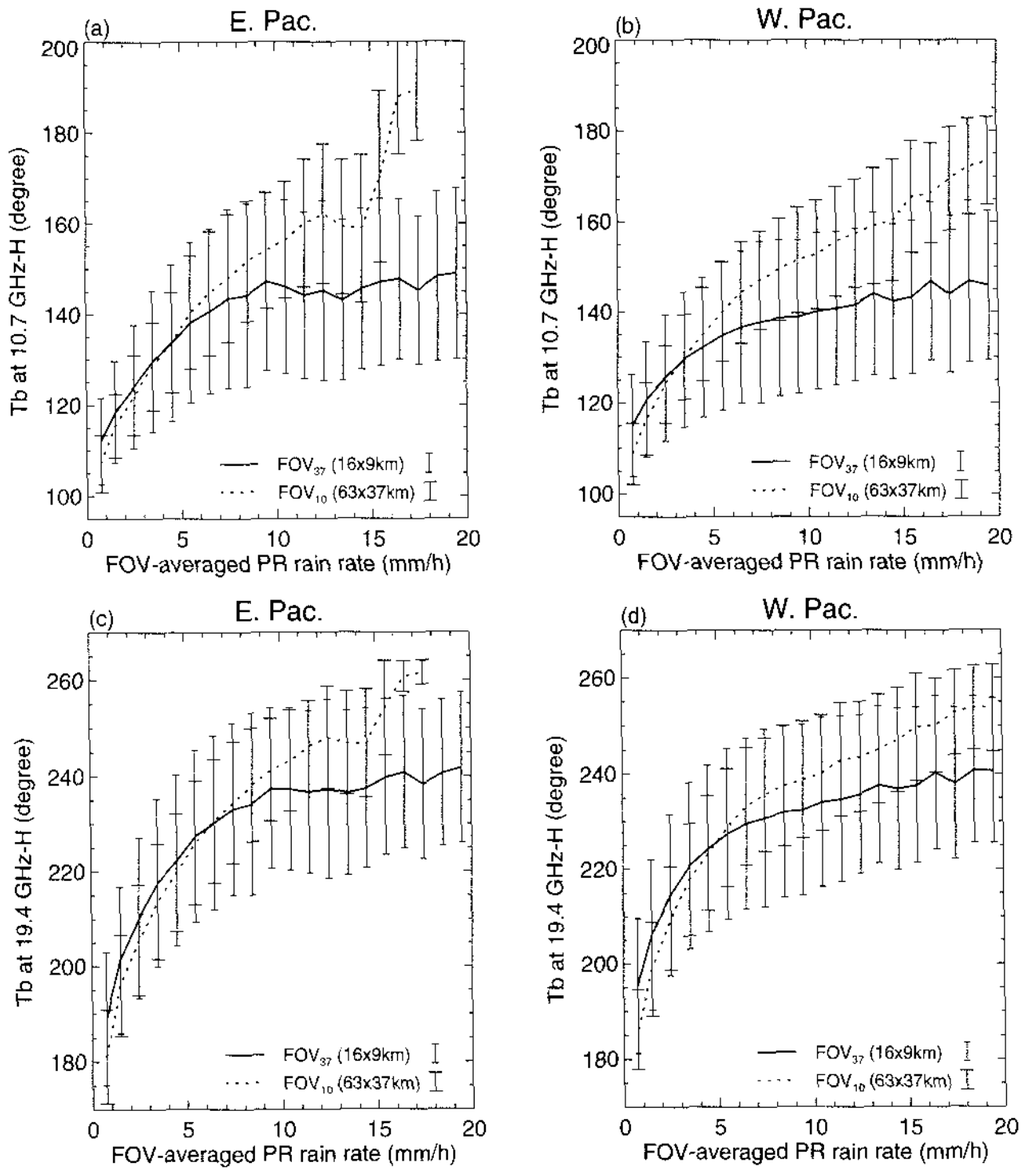

Figure 1. Relationships between T_b and R obtained at two different spatial resolutions, FOV_{37} (solid line) and FOV_{10} (dotted line) over the east and west Pacific. The 10.7 GHz-H T_b to R is shown in the upper

panels and the lower panels represent 19.4 GHz-H T_b to R relations. The error bars denote the ±1 standard deviations as before.

3. HIGH AND LOW RESOLUTIN RAINFALLS FROM OBSERVATION-BASED RETRIEVALS

Based on the fact that the radiometric signatures at the lower resolutions tend to maintain a greater dynamic range than at the higher resolutions, which is resulted from the different distribution of rainfall inhomogeneity with rain rates, this section retrieves rainfalls at low resolutions and compares the low resolution rainfall estimates to their counterparts at higher resolutions.

3.1 Observation-based retrieval algorithm

The retrieval algorithm does not include any complicated procedures to increase the retrieval performance, but a straightforward Bayesian inversion method is employed. The *a-priori* databases for the retrieval are computed separately by averaging the rainfall and T_b's of each channel over the retrieval resolutions as used in Figure 1. Once a database is generated, the inversion problem is resolved by the Bayesian methodology as used in SK. Similar Bayesian methodologies have been used (e.g. Olson et al. 1996, and Marzano et al. 1999). In this approach, the state vector **h** can be PR rain parameters and the measurement vector **b** will be the set of TMI brightness temperatures. The posterior probability, which is the object of the Bayesian inference, may be expressed as

$$P(\mathbf{h} \mid \mathbf{b}) \propto P(\mathbf{b} \mid \mathbf{h}) P(\mathbf{h}) \qquad (1)$$

where $P(\mathbf{b}|\mathbf{h})$ is the probability of **h** conditional on **b**. The conditional probability, $P(\mathbf{b} \mid \mathbf{h})$, may be modeled by a multi-dimensional Gaussian distribution of the difference between the observation and the modeled observation with the uncertainty given by the measurement and forward simulation. In the retrieval with the observation database, the error from the forward computations will not appear in the covariance matrix for the term $P(\mathbf{b}|\mathbf{h})$. The covariance matrix has only diagonal elements representing the instrumental noises at each channel. The retrievals are intended to compare the rainfall estimates at different retrieval resolutions such that the PR data, assumed as true rain rates, are averaged over the retrieval resolutions. Furthermore, since $P(\mathbf{h})$ of the prior information is a good description of the true probability distribution of precipitation fields, $P(\mathbf{h})$ is simply replaced by the frequency of each element in the prior information. That is, the database based on the three months of TRMM data is a good representation of distribution and variability of rain fields for the synthetic retrievals.

3.2 Comparisons of high and low resolution rainfall estimates

The rainfalls retrieved at the three different retrieval resolutions, FOV_{37}, FOV_{19}, and FOV_{10}, over the east Pacific during DJF, 1999-2000 are compared in Figure 2. Obviously, the bias, RMS errors and correlation between the PR and estimate rainfalls are consistently improved with lower retrieval resolutions due to the larger dynamic range and less variability in T_b-R relations. However, the direct comparison of the retrieval results for different resolutions is not appropriate because the high resolution retrieval itself has great benefits for observing the details of precipitation. Moreover, some important constraining information that can increase the retrieval performance significantly is not considered in the retrievals. As such detail comparison of the estimates from the different resolutions is not relevant to this study. We are mainly concern if the low resolution estimates can be achieved accurately if the appropriate information on T_b and R relations for the retrieval resolution is used.

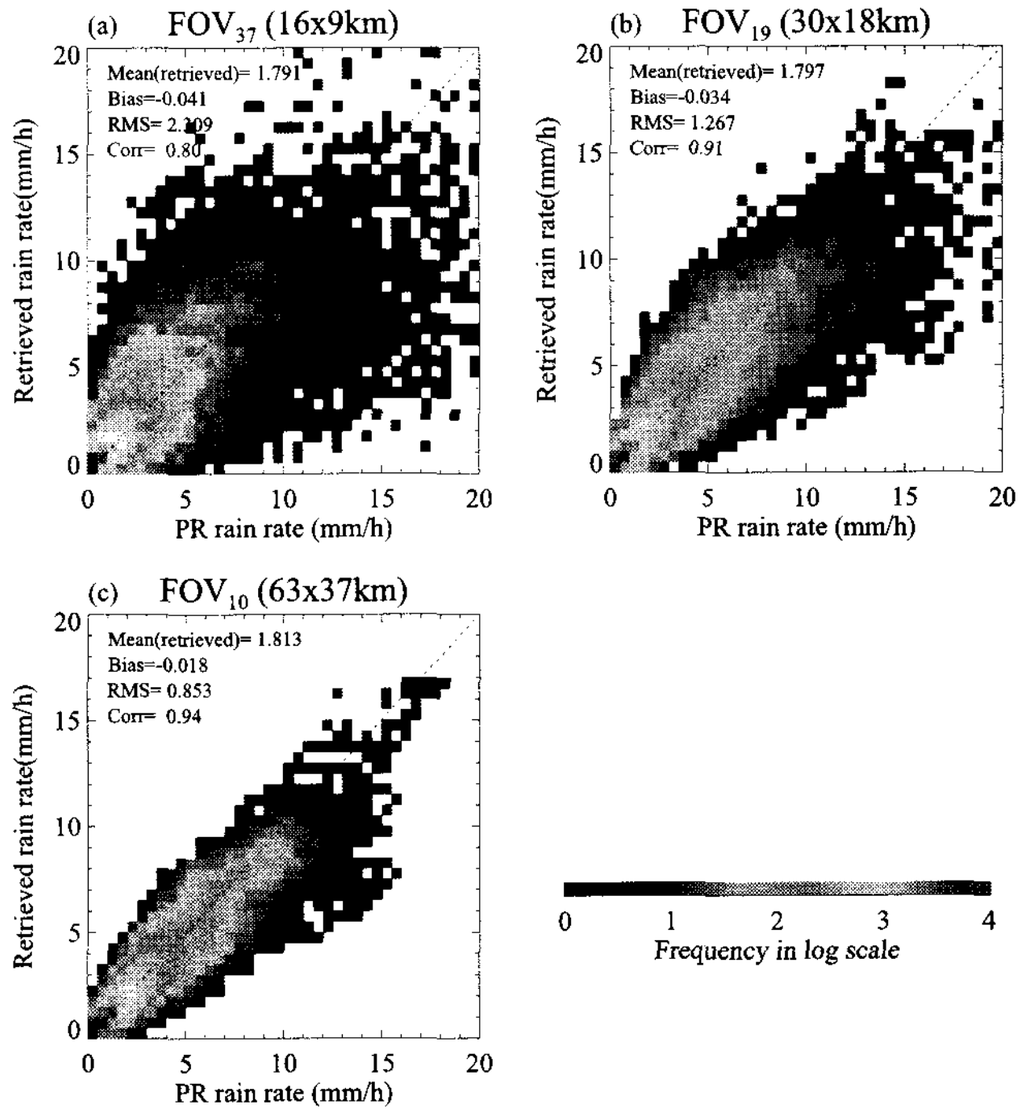

Figure 2.. Two-dimensional histograms showing the PR (as a truth) and estimated rain rates at different retrieval resolutions (FOV_{37}, FOV_{19}, and FOV_{10}). Retrievals are performed over the east Pacific during the period of DJF, 1999-2000. Color in square box indicates frequency in $\log_{10}$ scale.

The FOV_{19} and FOV_{37} rainfall estimates are also averaged at the resolution of FOV_{10} and compared them with the rain rates directly retrieved at FOV_{10}. In the averaging of the higher resolution estimates into FOV_{10}, about 16 pixels of FOV_{37} and about 4 pixels of FOV_{19}, which correspond approximately to the size of FOV_{10}, are used respectively. The retrieval statistics averaged from the higher resolutions (FOV_{37} and FOV_{19}) to FOV_{10}

are shown in the rows (a) and (b) of Table 1, respectively. The statistics corresponding to the rainfalls directly estimated at FOV_{10}, as already shown in Figure 2c, are presented in the row (c) as well for comparison.

As expected, averaging the higher resolution (FOV_{37} or FOV_{19}) estimates at the resolution of FOV_{10} does not change the bias statistics, but decreases the RMS error and increases the correlation (refer to the numbers in Figure 2a, b for the corresponding high resolution estimates). Meanwhile, the direct retrieval at the low resolution (FOV_{10}) shows better retrieval statistics. It results from the use of the *a-prior* database that is characterized by the higher degree of linearity and greater dynamic ranges in the T_b responses to rain rates at the larger spatial scale. Retrieval statistics for the west Pacific are also shown in Table 2. Similar results can be found over the west Pacific.

Table 1. Statistics of the rainfall estimates at the resolution of FOV_{10} for the east Pacific. The rainfalls at FOV_{37} and FOV_{19} are averaged over the resolution of FOV_{10} and are presented in the rows (a) and (b), respectively. The row (c) also shows the statistics of estimates directly performed at FOV_{10}. Numbers in parentheses represent percent value of the PR mean rain rate.

	Mean rain rate				
	PR	Estimated	Bias	RMS	Corr.
(a) Averaged from FOV_{37}	1.832	1.791	-0.041 (-2.237%)	1.194	0.89
(b) Averaged from FOV_{19}	1.832	1.798	-0.034 (-1.871%)	1.129	0.92
(c) FOV_{10}	1.832	1.813	-0.018 (-1.005%)	0.853	0.94

Table 2. Same as Table 1, but for the west Pacific.

	Mean rain rate				
	PR	Estimated	Bias	RMS	Corr.
(a) Averaged from FOV_{37}	1.894	1.871	-0.023 (-1.215%)	1.271	0.84
(b) Averaged from FOV_{19}	1.894	1.880	-0.014 (-1.744%)	1.332	0.88
(c) FOV_{10}	1.894	1.885	-0.010 (-0.508%)	1.185	0.90

4. CONCLUSIONS

This study has examined coincident TRMM TMI and PR data to construct distributions of rain rate statistics, such as the coefficient of variation CV. The impact of the rain rate statistics at various scales on the radiometric signatures is then investigated. Based on the observational characteristics a low resolution rainfall retrievals have been performed at the various spatial resolutions. The results shows that low resolution rainfall retrievals can be less affected by the rainfall inhomogeneity by including realistic rainfall distributions (resulting in the greater dynamic range in T_b responses) in its *a-priori* database. It suggests that even modest radiometers with low resolution FOV can contribute to more microwave rain samples that can be used in making more reliable climatological rainfalls from current or planned microwave sensors.

References:

Chiu, L. S., G. R. North, D. A. Short, and A. McConnell, 1990: Rain estimation from satellites: Effect of finite field of view. J. Geophy. Res., 28, 2177-2185.

W. S. Olson, and L. Giglio, 1996: A simplified scheme for obtaining precipitation and vertical hydrometeor profiles from passive microwave sensors. IEEE Trans. Geosci. Remote Sens., 34, 1213-1232.

Marzano, F. S., A. Mugnai, G. Panegrossi, N. Pierdicca, E. A. Smith, and J. Turk, 1999: Bayesian estimation of precipitating cloud parameters from combined measurements of spaceborne microwave radiometer and radar, IEEE Trans. Geosci. Remote Sens., 37, 596-613.

Olson, W. S., C. Kummerow, G. M. Heymsfield, and L. Giglio, 1996: A method for combined passive-active microwave retrievals of cloud and precipitation profiles. J. Appl. Meteor., 38, 1763-1789.

Shin, D.-B., and C. Kummerow, 2003: Parametric rainfall retrieval algorithms for passive microwave radiometers. J. Appl. Meteor., 42, 1480-1496.

Short, D. A., and G. R. North, 1990: The beam filling error in ESMR-5 observations of GATE rainfall. J. Geophys. Res., 95, 2187-2194.

Acknowledgements

This work was supported in part by Yonsei University Research Fund of 2007-1-0006.